PHYSICAL REVIEW B **74**, 235213 (2006)

Mn 3*d* electronic configurations in $(Ga_{1-x}Mn_x)As$ ferromagnetic semiconductors and their influence on magnetic ordering

F. Kronast,* R. Ovsyannikov, A. Vollmer, H. A. Dürr, and W. Eberhardt
BESSY, Albert-Einstein-Strasse 15, 12489 Berlin, Germany

P. Imperia and D. Schmitz
Hahn-Meitner-Institiut, Albert-Einstein-Strasse 15, 12489 Berlin, Germany

G. M. Schott, C. Ruester, C. Gould, G. Schmidt, K. Brunner, M. Sawicki,† and L. W. Molenkamp
Universität Würzburg, am Hubland, 97074 Würzburg, Germany

(Received 7 June 2006; revised manuscript received 19 October 2006; published 18 December 2006)

We applied x-ray absorption spectroscopy and x-ray magnetic circular dichroism (XMCD) at the Mn 2*p*-3*d* resonances to study the Mn 3*d* electronic configuration and the coupling of Mn 3*d* magnetic moments in various $Ga_{1-x}Mn_xAs$ films. The homogeneity of the Mn depth profile throughout the $Ga_{1-x}Mn_xAs$ film was tested by additional structure-sensitive x-ray resonant reflectivity measurements. In all investigated $Ga_{1-x}Mn_xAs$ films the electronic and magnetic configuration of the Mn impurities varies throughout the Mn-doped layer. This inhomogeneity is caused by the surface segregation of nonferromagnetic Mn in a d^5 configuration. X-ray resonant reflectivity data show that the accumulation of nonferromagnetic Mn near the surface is strongly enhanced by low-temperature annealing. By XMCD we identified the Mn species responsible for the long-range ferromagnetic coupling. It is characterized by an Mn $3d^5$-$3d^6$ mixed-valence acceptor state that is unchanged at all investigated Mn concentrations, ranging from 1% to 6%. Additional nonferromagnetic Mn occurs in the bulk of high-concentration samples. We discuss a model in which the latter is due to antiferromagnetic Mn-Mn nearest-neighbor pairs.

DOI: 10.1103/PhysRevB.74.235213 PACS number(s): 78.70.Dm, 75.50.Pp, 75.30.Hx, 75.30.Et

I. INTRODUCTION

Carrier-induced ferromagnetism in III-V-based dilute semiconductors such as $(Ga_{1-x}Mn_x)As$ makes these materials promising candidates for spintronics applications. The ferromagnetism in $Ga_{1-x}Mn_xAs$ is based on two cooperative effects caused by replacing Ga atoms with Mn. Mn provides a local spin-5/2 magnetic moment, and as an acceptor it creates itinerant holes, which mediate the long-range ferromagnetic order.[1]

However, the origin of ferromagnetism in these materials is not well understood. This is reflected in the different Mn 3*d* electronic configurations and their influence on exchange coupling reported in the literature. Most models of exchange coupling presently discussed are based on a localized Mn $3d^5$ electronic configuration that interacts with holes via impurity states consisting of mainly Ga/As 4*sp* orbitals.[2–4] Population analysis indicates that the number of Mn 3*d* electrons is actually between $3d^5$ and $3d^6$ (Ref. 5). However, there are also experimental reports that Mn is present in a $3d^4$ configuration.[6] In Ref. 6 the $3d^4$ component was even considered essential to establish ferromagnetic order. Due to the limited solubility of Mn, the presence of defects such as interstitial Mn also has to be considered.[7] The formation of As antisite defects and interstitial Mn was predicted. Both defects should act as double donors partially compensating the effect of the Mn acceptors.[7] Furthermore, it was proposed that interstitial Mn tends to align antiferromagnetically with substitutional Mn effectively canceling their moments.[8] The presence of Mn interstitials close to clusters of substitutional Mn was also predicted to strongly modify the exchange coupling between the latter as well as their charge state.[9,10] Finally, in contrast to II-VI-based magnetic semiconductors no antiferromagnetic exchange between Mn-Mn nearest neighbors has been considered for (GaMn)As due to a lack of experimental evidence despite its possibly adverse effect on a high ferromagnetic T_c (Ref. 11).

For the understanding of the ferromagnetic ordering the electronic configuration of the Mn impurities and the number of Mn atoms contributing to the long-range ferromagnetic order are of major interest. These parameters can be probed directly by x-ray absorption spectroscopy (XAS) and x-ray magnetic circular dichroism (XMCD). At the Mn $2p^63d^n \rightarrow 2p^53d^{n+1}$ resonance the XAS and MXCD line shapes are characteristic for the Mn 3*d* electronic and magnetic configurations, respectively.[12] The contribution of magnetic and nonmagnetic 3*d* states to the x-ray absorption process can be separated by using the difference (XMCD) and sum (XAS) of spectra taken with opposite x-ray helicities. Although these techniques have been applied to $(Ga_{1-x}Mn_x)As$ previously,[13–17] the results are in some points inconsistent. The first experiments[13,14] found a pronounced multiplet structure in the Mn XAS spectra characteristic of a highly localized state. The weak XMCD signal indicated that only a fraction of 13% of the Mn atoms participate in the long-range ferromagnetic ordering. Changes in the line shape of the Mn XAS spectra before and after annealing have been observed, indicating that more than one Mn component must be present in $(Ga_{1-x}Mn_x)As$ (Ref. 15). More recently XAS spectra with less pronounced multiplet structure have been reported[16] in combination with a remarkably high number (66%) of ferromagnetically aligned Mn impurities in

$(Ga_{1-x}Mn_x)As$ (Ref. 16). It has been proposed very recently[17] that this discrepancy may be caused by a Mn-rich surface layer.

We applied XAS and XMCD techniques to $(Ga_{1-x}Mn_x)As$ films with different Mn concentrations in order to study the Mn $3d$ electronic configurations of Mn impurities in the GaAs host lattice and their influence on the ferromagnetic exchange coupling. The different probing depth of total electron yield and total fluorescence yield was used to distinguish between bulk and surface properties. At all Mn concentrations we find the bulk dominated by Mn impurities in a mixed valence $3d^5$-$3d^6$ electronic configuration. This has been assigned to substitutional Mn hybridizing with the GaAs host.[13] For low Mn concentrations the magnetic moments of substitutional Mn can be completely aligned in an external magnetic field. At high Mn concentrations a reduced saturation magnetization of substitutional Mn indicates the presence of antiferromagnetic coupling between substitutional Mn. At the surface we observe substitutional Mn and a second Mn species in a localized $3d^5$ configuration. The contributions of both Mn species to the spectra are clearly discernible by their different multiplet structure and a 0.6-eV core-level shift of the $2p$-$3d$ resonance. Depth profiles of the two Mn species, obtained by resonant reflectivity measurements, demonstrate that segregation of Mn $3d^5$ leads to the formation of a surface layer in all samples. An enhanced Mn $3d^5$ concentration in the surface layer after 24 h of low-temperature annealing indicates that its formation is related to the diffusion of interstitial Mn. In the surface layer containing nonferromagnetic Mn $3d^5$ the ferromagnetic coupling between substitutional Mn is strongly reduced compared to the bulk.

The paper is organized as follows: After describing the experimental details we present the bulk and surface properties of different $Ga_{1-x}Mn_xAs$ layers. In Sec. III B we study the chemical depth profile of the $Ga_{1-x}Mn_xAs$ layers by resonant reflectivity. This allows us to investigate the distribution of different Mn species and its influence on the ferromagnetic coupling. In Sec. III C we demonstrate the presence of an additional nonferromagnetic Mn species with an electron count close to $3d^4$ at high Mn concentrations. We discuss a model in which the latter is due to Mn-Mn antiferromagnetic nearest-neighbor pairs.

II. EXPERIMENTAL SETUP AND SAMPLE PREPARATION

The investigated $Ga_{1-x}Mn_xAs$ films were grown on a GaAs (001) surface by low-temperature molecular beam epitaxy[18] (MBE). A 80-nm-thick low-temperature GaAs buffer layer was deposited below the Mn-doped layer. In this paper we present results obtained from four samples with Mn concentrations of $x=0.007$, 0.017, 0.051, and 0.062. The thickness of the Mn-doped layer was 350, 300, 500, and 180 nm, respectively. The rms roughness of the surface was 0.6 ± 0.2 nm as detected by atomic force microscopy (AFM). We assign this roughness to thickness variations of the $Ga_{1-x}Mn_xAs$ layer. On a longer lateral length scale of 200–400 nm the AFM data reveal an additional corrugation of the surface with an amplitude of 8 ± 3 nm. The latter corrugation is caused by thickness variations of the low-temperature GaAs buffer layer and was observed in all samples except for the $x=0.062$ sample. The $x=0.062$ sample was studied in the as-grown state and after annealing to 185 °C for 24 h under vacuum.

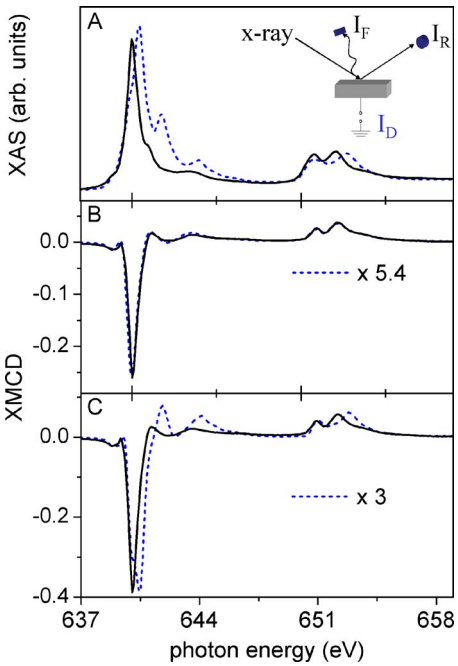

FIG. 1. (Color online) (A) shows the normalized XAS spectra of the as-grown $(Ga_{1-x}Mn_x)As$ film with $x=0.062$. They were recorded at x-ray incidence of $\Theta=23°$ using fluorescence yield (solid black line) and total electron yield (dashed blue line) detection. (B) shows the corresponding XMCD spectra in remanence and (C) at an external field of 2.5 T applied along the photon incidence direction. The inset shows a schematic view of the experiment with simultaneous detection of fluorescence I_F, reflection I_R, and total electron yield I_D signals.

The inset of Fig. 1(A) shows a schematic view of the experiment. We used photodiodes to measure the reflectivity signal I_R and the fluorescence yield I_F. The total electron yield was obtained from the sample drain current I_D. All signals were recorded simultaneously. Parts of the measurements were carried out in a superconducting magnet at external magnetic fields up to 4.5 T. In remanence a permanent field of 0.005 T was applied to align the magnetization along the in-plane hard axis of the samples. The Mn $2p$ XMCD spectra were recorded at the beamline UE46-PGM at BESSY and at ID8 at the ESRF. XMCD was measured as the difference between x-ray absorption spectra taken with opposite light helicities. The XAS spectra shown below correspond to the sum spectra of the two opposite x-ray helicities. The degree of circular polarization was 95% at BESSY and 100% at the ESRF.

III. RESULTS

A. Bulk versus surface properties

At the surface of all $Ga_{1-x}Mn_xAs$ films we find Mn $3d$ electronic configurations that deviate strongly from those of

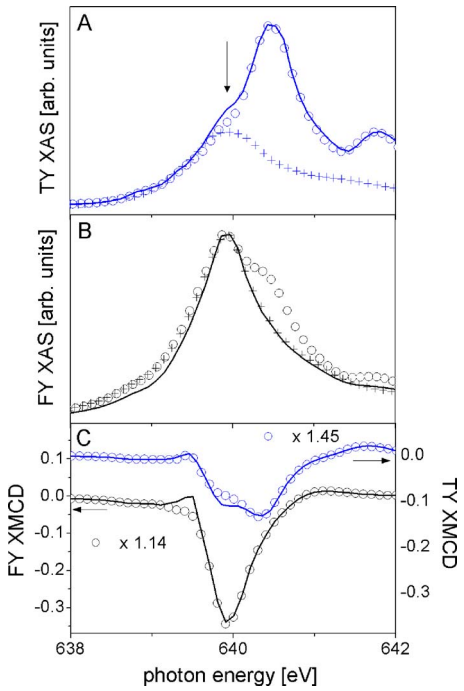

FIG. 2. (Color online) (A) Surface-sensitive total electron yield (TY) XAS and (B) bulk-sensitive total fluorescence yield (FY) XAS spectra of the $x=0.062$ sample. The displayed spectra were recorded in the as-grown state (solid line), after 24 h of annealing (open circles), and with the surface layer removed by Ar-ion sputtering (crosses). (C) XMCD spectra corresponding to the as-grown state (lines) and after annealing (symbols), recorded at 2.5 T external magnetic field applied along the photon incidence direction. The XMCD spectra recorded in fluorescence yield and electron yield are offset for clarity.

the bulk. This becomes evident if we compare XAS and XMCD spectra recorded with the surface-sensitive total electron yield to those recorded with the bulk sensitive fluorescence yield detection as shown in Fig. 1. The displayed spectra were taken at the Mn $2p$-$3d$ resonance and display two pronounced edges due to transitions into localized $3d$ states producing $2p_{3/2}$ and $2p_{1/2}$ core holes. XAS spectra are normalized to a constant-step-like background caused by transitions into continuum states. The XAS multiplet structure obtained with bulk-sensitive fluorescence yield is very different from that seen with surface-sensitive total electron yield detection [Fig. 1(A)]. In addition the $2p$-$3d$ resonance maximum in total electron yield is shifted to 0.6 eV higher photon energy compared to the fluorescence spectrum. In contrast the XMCD line shape in remanence is very similar for both detection methods as shown in Fig. 1(B). With an applied field of 2.5 T the asymmetry of the bulk XMCD spectra (i.e., the difference of two XAS spectra taken with opposite helicity divided by their sum) increases from $27\% \pm 2.2\%$ to $39\% \pm 2.2\%$. The line shape remains identical to the spectrum taken at remanence. In the surface-sensitive XMCD spectra a second peak appears with the applied field as shown in Fig. 1(C). The second peak is shifted to 0.6 eV higher photon energy compared to the XMCD spectrum recorded at remanence, and it corresponds to the $2p$-$3d$ resonance maximum in total electron yield XAS [see Fig. 1(A)]. The XMCD asymmetry obtained by surface-sensitive total electron yield is much lower than that for bulk fluorescence yield.

Low-temperature annealing in vacuum (24 h at 185 °C) which is thought to at least partially remove interstitial Mn from the bulk by diffusion processes[19] leads to changes in the XAS and XMCD spectral line shape. This is demonstrated in Fig. 2, where spectra for the $x=0.062$ sample before (symbols) and after (lines) annealing are shown. With total electron yield we find a reduced intensity for the low-photon-energy shoulder of the XAS spectrum after annealing [see arrow in Fig. 2(A)]. This shoulder corresponds to the main XAS peak observed in the bulk-sensitive fluorescence yield detection [see Fig. 2(B)]. Similar changes are also visible in the total electron yield XMCD spectra recorded for an applied field of 2.5 T [see Fig. 2(C)]. The shoulder corresponding to the bulk XMCD spectrum is reduced in intensity by annealing. In addition the maximum asymmetry is reduced by a factor of 1.45 as shown in Fig. 2(C). In the fluorescence yield spectra an additional multiplet structure appears in the XAS spectra of the annealed sample [see Fig. 2(B)]. This structure is identical to the one observed with electron yield. It is absent in the spectra after removing the surface layer by Ar-ion sputtering [crosses in Fig. 2(B)]. Interestingly the additional multiplet structures in fluorescence do not contribute to the XMCD signal. The XMCD spectra recorded in fluorescence before and after annealing have almost identical line shapes. This means the additional structures occurring in the fluorescence yield XAS correspond to nonferromagnetically ordered Mn. The XMCD asymmetry in fluorescence is reduced by about $12\% \pm 2\%$ in the annealed spectrum.

XAS and XMCD line shapes at the $2p$-$3d$ resonance are characteristic of the $3d$ valence configuration.[12] The very different XAS line shapes in Figs. 1 and 2, therefore, point to different Mn species in the bulk and at the surface of the $Ga_{1-x}Mn_xAs$ films. The changes of the spectral line shape upon annealing and after removing the surface by Ar-ion sputtering allow us to identify the line shapes of the contributing Mn species. After sputtering the surface layer the total electron yield spectrum becomes very similar to the bulk-sensitive fluorescence yield spectrum. Thus we can decompose the total electron yield XAS spectrum of Fig. 2(A) assuming that the shoulder at a photon energy of 640 eV is caused by contributions from the Mn species present in the bulk. Such an assignment is strengthened by the identical XMCD line shape observed in both detection channels at remanence [see Fig. 1(B)]. Accordingly we also have to decompose the total electron yield XMCD spectrum recorded at 2.5 T external magnetic field since only in the surface-sensitive spectrum does an external magnetic field cause a change in the line shape. This decomposition implies that the low-photon-energy shoulder in the total electron yield XMCD spectrum [see Fig. 2(C)] is caused by contributions from the Mn species dominating the bulk. The results of this analysis are displayed in Figs. 3(A) and 3(C). The XAS and XMCD line shapes of the surface species agree with multiplet calculations for a $3d^5$ electronic configuration.[12] The reference spectra shown in the insets of Figs. 3(A) and 3(C) were calculated by van der Laan and Thole for Mn $d5$ in

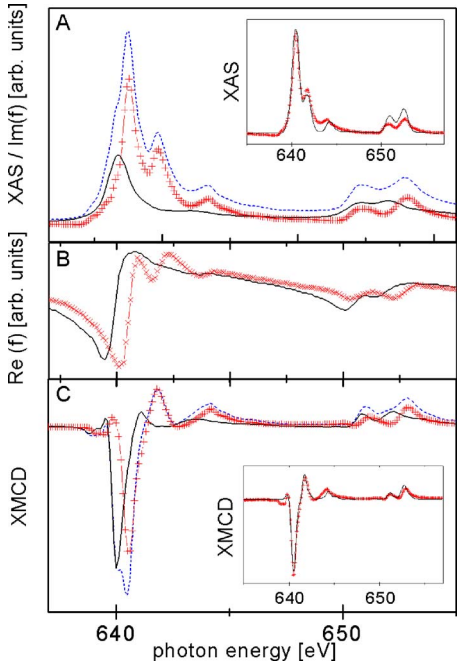

FIG. 3. (Color online) (A) Decomposition of the electron yield XAS spectrum of the as-grown $x=0.062$ sample (dashed line) into Mn_I (solid line) and Mn_{II} (crosses) contributions as described in the text. The spectra correspond to the imaginary part of the scattering amplitude f. The comparison between the Mn_{II} (crosses) line shape and a calculated Mn $3d^5$ XAS spectrum (Ref. 12) (black lines) is shown in the inset. (B) Real part of the scattering amplitude f derived via Kramers-Kronig transformations from Im(f). (C) XMCD electron yield spectrum recorded at 2.5 T external field containing contributions of Mn_I (solid line) and Mn_{II} (crosses) separated in the individual spectra. The inset shows a comparison between the Mn_{II} (crosses) line shape and a calculated Mn $3d^5$ XMCD spectrum (Ref. 12).

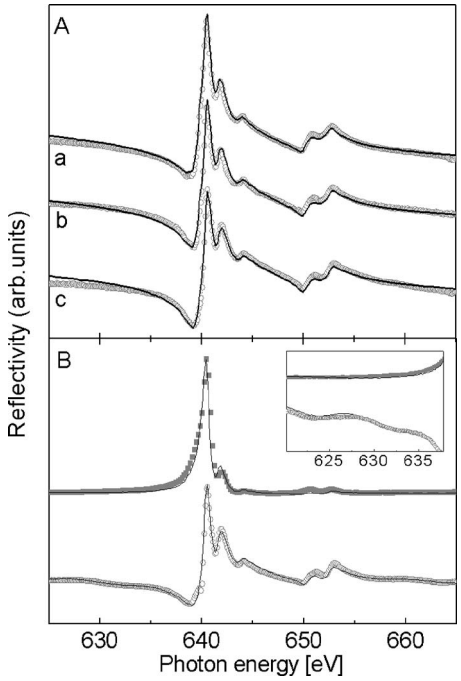

FIG. 4. (A) X-ray resonant reflectivity spectra of the $x=0.0175$ sample (open circles) recorded at incidence angles of $a=63°$, $b=67°$, and $c=71°$. The fits to the spectra are shown as black lines. (B) Reflectivity spectra of the $x=0.062$ sample before (open circles) and after (solid squares) annealing. The fits to the spectra are shown as black lines. The inset shows the enlarged pre-edge part of the spectra.

spherical symmetry (no crystal field applied).[12] We note that no other decomposition gives a similar agreement. In the following the Mn species dominating the bulk will be denoted as Mn_I and Mn $3d^5$ will be denoted as Mn_{II}.

B. Chemical depth profile

In the next step we can use the separated XAS line shapes of Mn_I and Mn_{II} to investigate their distribution throughout the $Ga_{1-x}Mn_xAs$ films by x-ray resonant reflectivity measurements. The reflectivity is given by

$$I \propto \left| \sum_i f_i \exp(i\mathbf{q} \cdot \mathbf{r}_i) \right|^2, \qquad (1)$$

where f_i is the complex scattering amplitude of the atom i at the position $\mathbf{r}_i$ and $\mathbf{q}$ the scattering vector. The Mn_I and Mn_{II} XAS spectra shown in Fig. 3(A) correspond to the imaginary parts of the scattering amplitude, Im(f), of the respective Mn species. The real part Re(f), shown in Fig. 3(B), was calculated by Kramers-Kronig transformation of Im(f). The different line shape of Re(f) and Im(f) implies a phase shift between incident and scattered x rays. The phase shift depends on the chemical composition of the individual layers and leads to interferences as a function of $\mathbf{q}$—i.e., the incidence angle and the photon energy. Due to the presence of these interference effects, the line shape of the reflectivity spectra differs from the XAS spectra and varies with the incidence angle. This is shown for the $x=0.017$ sample in Fig. 4(A). With an increasing incidence angle we observe a decreasing resonance peak height and the increase of a dip on its low-energy side in the reflectivity spectrum. More dramatic changes occur if we compare the reflectivity spectra of the $x=0.062$ sample before and after 24 h of low-temperature annealing as shown in Fig. 4(B). As will be shown below these changes result from a change of the thickness of the surface layer, which is also indicated by the change of the XAS spectra recorded by fluorescence and electron yield upon annealing.

To resolve the chemical depth profile we used Eq. (1) to fit the reflectivity curves by a model structure. The calculations were done employing the IMD code,[20] which is based on a modified Fresnel coefficient formalism.[21] The measured reflectivity spectra were modeled by dividing the sample into three layers as shown in the inset of Fig. 6(A) below: (i) the low-temperature GaAs substrate with semi-infinite thickness, (ii) the bulk $Ga_{1-x}Mn_xAs$ layer with given thickness and Mn_I concentration, and (iii) a surface layer with variable thickness and concentrations of Mn_{II} and Mn_I. Input parameters in our model are the bulk Mn_I concentration, the thickness of the $Ga_{1-x}Mn_xAs$ layer, the interface roughness, and the scattering amplitudes of Mn_I and Mn_{II}. As fit parameters we used the thickness of the surface layer and the concentrations of Mn_I and Mn_{II} in the surface layer.

For the $x=0.062$ sample we determined the thickness and the interface roughness of the $Ga_{1-x}Mn_xAs$ layer directly. In the absence of any interface corrugation the finite thickness of the $Ga_{1-x}Mn_xAs$ layer causes the interference fringes visible in the inset of Fig. 4(B) as intensity oscillations. From the fit we find a interface roughness of 0.65 ± 0.1 nm in the as-grown state in perfect agreement with the 0.6 ± 0.2 nm obtained by atomic force microscopy. After annealing these oscillations disappear. This effect can only be reproduced in our model if we assume that the interface region between $Ga_{1-x}Mn_xAs$ and low-temperature GaAs broadened to more than 3 nm by diffusion of Mn into the buffer layer. The line shape changes after annealing are reproduced by our model for an increase of the thickness of the surface layer and its Mn_{II} concentration. This is consistent with the total electron and fluorescence yield XAS spectra displayed in Figs. 2(A) and 2(B), respectively. In the annealed total electron yield spectrum (open circles) the shoulder (marked by the arrow) corresponding to the Mn_I $2p$-$3d$ resonance peak is less pronounced. In the annealed fluorescence spectrum (open circles) a high-photon-energy shoulder corresponding to the Mn_{II} $2p$-$3d$ resonance appears. Upon annealing the ratio between Mn_I and Mn_{II} at the surface has changed and the total amount of Mn_{II} in the surface region increases.

C. Bulk magnetization

We will now focus on the bulk properties of the $Ga_{1-x}Mn_xAs$ films. To avoid any influence of the surface layer we removed the surface layer by Ar-ion sputtering previous to these measurements. We will discuss only fluorescence data in the following. Figure 5 displays bulk XAS and XMCD spectra of the $Ga_{1-x}Mn_xAs$ films with the lowest and highest Mn concentrations ($x=0.007$ and $x=0.062$). Interestingly their XMCD line shapes are identical. Only the as-grown $x=0.062$ XMCD spectrum displays a minor line shape change at the pre-edge of the L_3 peak which, however, disappears after annealing [see Fig. 2(C)]. The bulk saturation magnetization depends strongly on Mn concentration. Magnetization curves versus applied magnetic field for the different Mn concentrations are shown in the inset of Fig. 5(B). The hysteresis loops were taken at a sample temperature of 8 K, and for $x=0.007$ and 0.017 they show signs of coexisting ferromagnetic and paramagnetic regions. With increasing Mn concentration T_C increases and the ferromagnetic regions develop into percolation networks eventually covering the whole sample at $x=0.062$. This behavior is also reflected in an increase of XMCD intensity with x at remanence shown in Fig. 6(C). The relative saturation magnetization obtained from the hysteresis loops at fields when all ferromagnetic and paramagnetic Mn moments are aligned is plotted in Fig. 6(D) (circles). It shows a significant reduction with increasing Mn content for the as-grown samples (solid circles). A further reduction by $12\%\pm2\%$ occurs with annealing of the $x=0.062$ sample (open circle). Contrary to the XMCD the XAS line shape changes significantly with increasing Mn concentration, especially at the low-photon-energy side of the L_3 edge. This effect seems to be influenced by the presence of defects like interstitial Mn since the XAS line shape

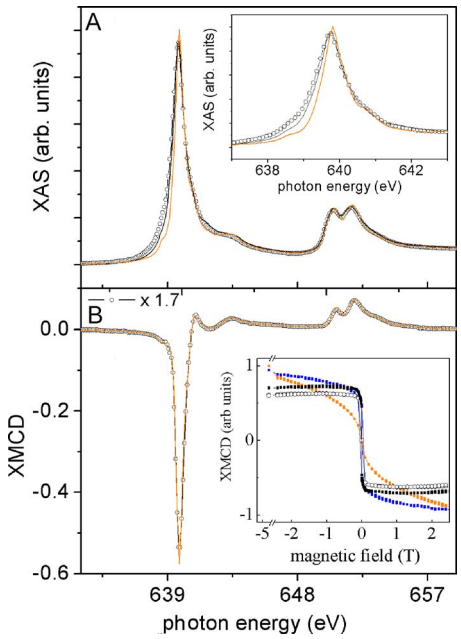

FIG. 5. (Color online) (A) XAS spectra from the as-grown $x=0.007$ (orange line) and the as-grown (black line) and annealed (open circles) $x=0.062$ samples. The associated XMCD spectra for the as-grown $x=0.007$ (orange line) and the annealed (open circles) $x=0.062$ samples are shown in (B). The spectra were recorded in magnetic saturation at 15 K. Note that for $x=0.062$ the XMCD intensity is rescaled by a factor of 1.7. The $x=0.017$ spectra (not shown) were identical to the $x=0.007$ case. The inset shows the XMCD signal at a photon energy of 640 eV probing the sample magnetization versus applied magnetic field for as-grown $(Ga_{1-x}Mn_x)As$ samples with $x=0.007$, 0.017, and 0.062 (solid orange, solid blue, and solid black symbols) and the annealed $x=0.062$ sample (open circles). All spectra were taken at 8 K, which is only slightly below T_C for the $x=0.007$ sample.

changes with annealing as visible in Figs. 2(B) and 5(A). We note that similar XAS line shape changes have been recently reported in Ref. 22 corroborating our results. Although no explanation of this effect was given in Ref. 22, it excludes extrinsic effects due to a possibly different sample preparation by different groups.

IV. DISCUSSION

The experimental results are summarized in Fig. 6. Panels (A) and (B) contain results from the reflectivity measurements, while panels (C) and (D) summarize the XMCD results. The XAS and reflectivity measurements clearly show the formation of a surface layer in the $Ga_{1-x}Mn_xAs$ films with electronic and magnetic properties strongly different from the bulk. The additional Mn species that only exists in the surface layer is characterized by a $3d^5$ electronic configuration. It is tempting to relate the second observed Mn species Mn_{II} to interstitial Mn. The growth process is known to provide pathways for the generation of interstitial Mn (Ref. 9); i.e., the concentration of interstitial Mn at the surface should be significantly higher. Diffusion of interstitial Mn from bulk to the surface during annealing has been

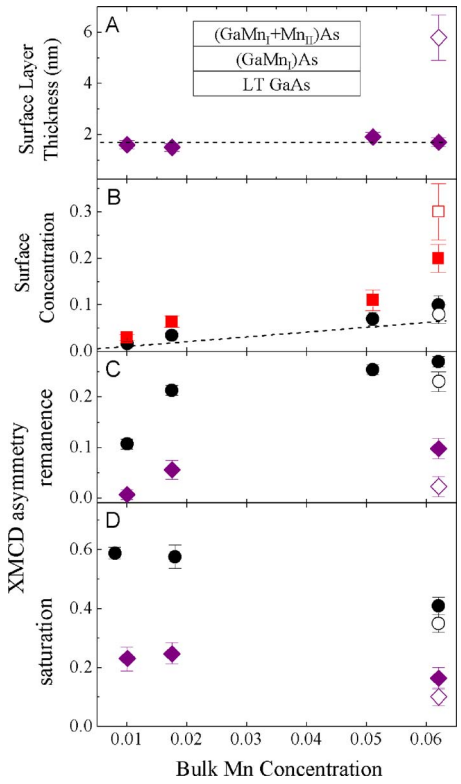

FIG. 6. (Color online) Summary of results for all samples shown as a function of Mn concentration. The sample structure is shown schematically in the inset. Solid symbols refer to the as-grown, open symbols to the annealed samples. (A) displays the thickness of the surface layer containing Mn_{II}. (B) shows the concentrations of Mn_I (circles) and Mn_{II} (square) in the surface layer derived from fits to the reflectivity signal. The lower two panels show the Mn_I XMCD asymmetry in the bulk (triangles) and at the surface (diamonds) normalized to the Mn_I bulk concentration. The values in (C) are obtained in remanence, and in (D) the sample was saturated by an external magnetic field along the in-plane direction.

observed.[19] This is consistent with the increased accumulation of Mn_{II} at the surface of our sample after annealing. Assuming that the accumulation of Mn_{II} at the surface is due to diffusion of interstitials out of the bulk, we can estimate that $5\% \pm 1\%$ of interstitial Mn was present in the bulk of the as-grown sample. Such an amount of material is less than the value of 17% recently obtained from ion channeling measurements.[23] However, the number of interstitial Mn atoms in the bulk may strongly depend on the growth conditions. Our reflectivity data indicate that during the vacuum annealing Mn diffuses not only to the surface but also into the substrate. It was reported previously[17] that the Mn_{II} line shape should be influenced by surface oxidation. Oxidation may cause the different magnetic configuration of the Mn_{II} atoms. The outer Mn_{II} atoms accessible to the electron yield carry a paramagnetic moment. However, the buried Mn_{II} atoms visible in the fluorescence yield after annealing show no sign of a paramagnetic moment or are strongly antiferromagnetically ordered even at a 2.5 T external magnetic field. This and the coexistence of ferromagnetically ordered Mn_I at the same depth below the surface indicates that the surface layer is not completely oxidized. The consistently higher surface concentration of Mn_I points to possible site exchanges of Mn_{II} atoms onto Mn_I sites. It has been shown that site exchanges between interstitial and substitutional Mn are energetically only favorable at nonequilibrium conditions during the growth process.[9] This is consistent with our observation that post-growth annealing produces hardly any change in the Mn_I surface species [open and solid circles in of Fig. 6(B)].

In all samples we observe the same bulk Mn_I XMCD line shape that also contributes to the surface spectra recorded in remanence. It is characteristic for a high-spin $3d^5$ ground state configuration with a small $3d^6$ admixture.[13] The characteristic $3d^5$ atomic multiplet is still discernible as peaks in the XMCD and the XAS spectra of Fig. 1 but the structures are attenuated by the $3d^6$ ground-state weight.[13,17] The latter is caused by hybridization of Mn $3d$ and ligand Ga/As $4sp$ states. It is characterized by an extra Mn $3d$ electron and a hole on the ligand atoms. Delocalized ligand holes mediate the ferromagnetic exchange between localized Mn impurities in dilute magnetic semiconductors.[11] For a high-spin $3d^5$ configuration only an extra electron with opposite spin orientation can be accommodated.[24] Therefore, the $3d^6$ weight leads to antiferromagnetic alignment between Mn and As magnetic moments as observed in Ref. 25. The mixed-valence $3d^5$-$3d^6$ configuration is characterized by an average number of $n=5.2$ Mn $3d$ electrons on all sites.[13] Similar values of $n=5.3$ and 5.1 were obtained from photoemission measurements and cluster model calculations[26] and XAS data (see below).[17] The unaltered XMCD line shape at all Mn concentrations demonstrates an identical local Mn $3d$ electronic configuration of the ferromagnetic Mn species.[13,24] It also implies that the local magnetic moments are identical for the ferromagnetic Mn species at all concentrations. Together with the reduced XMCD signal at saturation this shows that the fraction of Mn atoms participating in the long-range ferromagnetic order is reduced at larger concentrations. Part of this effect could be caused by noncollinear arrangements of Mn magnetic moments due to a RKKY-like magnetic interaction.[27] However, since the Mn XMCD line shape is known to be very sensitive to changes in the magnetic exchange coupling[24] the latter effect should play a minor role. The presence of Mn interstitials in the as-grown $x=0.062$ sample causes a slightly different XMCD line shape. This is an indication that substitutional and interstitial Mn occupy neighbor sites and form magnetic clusters.[10,8]

The bulk XAS line shape changes significantly with increasing Mn concentrations [see Fig. 5(A)]. At low Mn concentrations of $x=0.007$ and 0.017 the Mn $3d$ electronic configuration fluctuates mainly between $3d^5$ and $3d^6$ with an average $3d$ electron count at all Mn sites near $n=5.1$ (Ref. 17) or 5.2 (Ref. 13). We note that the XAS and XMCD line shapes cannot be reproduced by an incoherent superposition of $3d^5$ and $3d^6$ configurations.[28] This implies that all Mn atoms have the same mixed valence $3d^5$-$3d^6$ ground state and there is no phase separation, e.g., in $3d^5$- and $3d^6$-like Mn sites. The asymmetric broadening of the XAS line shape at higher Mn concentration can only be explained by the presence of a second Mn species with a different $3d$ configuration that contributes only to the asymmetrically broadened

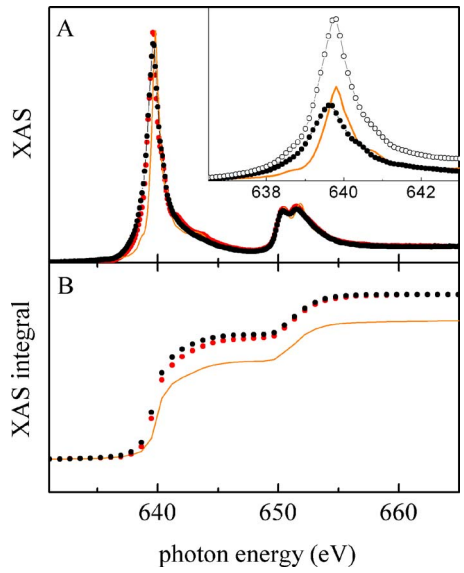

FIG. 7. (Color online) XAS spectra representing ferromagnetic (orange lines) and nonferromagnetic Mn species for as-grown (red circles) and annealed $x=0.062$ (black circles). The inset illustrates the decomposition of the annealed $x=0.062$ XAS spectrum (open circles) as described in the text. (B) Integral of the XAS spectra in (A) after subtraction of a steplike background (Ref. 24). The integral intensity corresponds to the number of unoccupied Mn 3*d* states for the respective species.

XAS line shape. This second species must be nonferromagnetic, causing the reduced saturation magnetization as displayed in Fig. 6(D). We can, therefore, separate the XAS line shape of ferromagnetic and nonferromagnetic Mn species. Figure 7 shows the decomposition of the XAS spectra for the $x=0.062$ sample in the as-grown and annealed state into spectra for nonferromagnetic (red circles and black circles) and ferromagnetic Mn species (orange lines). The line shape of the XAS spectrum for the ferromagnetic species was assumed to be identical to that of $x=0.007$. Its intensity was rescaled according to the measured XMCD ratios for $x=0.007$ and $x=0.062$ as shown in the inset (orange line). This corresponds to the fraction of ferromagnetically aligned Mn atoms in the sample. The line shapes of the resulting XAS spectra of the nonferromagnetic Mn species for as-grown (red circles) and annealed (black circles) $x=0.062$ samples are identical. This lends credibility to the quality of the decomposition procedure. We note that this line shape change cannot be caused by a phase separation and the formation of MnAs clusters as reported in Ref. 29. MnAs is known to display a large chemical shift and a significantly different line shape[16] than the one observed in Fig. 1.

The observed XAS line shape of nonferromagnetically coupled Mn_I displays much less pronounced multiplet features than that of the ferromagnetic species. Such an effect is characteristic for increased valence electron fluctuations[24,30] possibly due to increased electronic hopping between 3*d* shells of adjacent Mn-Mn pairs. A detailed line shape analysis similar to the $3d^5$-$3d^6$ Mn species is beyond the scope of the present paper. However, we can extract information about the ground-state properties using the integral XAS intensities after subtracting a steplike background[24] shown in Fig. 7(B). Sum rules relate the total $L_{3,2}$ intensity to the average number of unoccupied 3*d* levels, $n_h=10-n$.[13,17,24,30] For the nonferromagnetic species we find a 20%-reduced 3*d*-electron count close to $3d^4$ (Ref. 31) compared to that of ferromagnetic Mn atoms. Interestingly there is hardly a change in the branching ratio $BR=I(L_3)/[I(L_3)+I(L_2)]$ of the integral $L_{3,2}$ intensities $I(L_{3,2})$. We find BR values of 0.72 ± 0.01 and 0.75 ± 0.01 for the ferromagnetic and nonferromagnetic Mn species, respectively. Branching ratios so much larger than the statistical value of 2/3 are typical for high-spin ground-state configurations.[24,32] This result together with the zero XMCD spectrum is evidence that the $3d^4$-like Mn species is present as clusters with their high-spin atomic magnetic moments compensated by antiferromagnetic coupling.

Ferromagnetism is connected only to the d^5-d^6 Mn. In this case the exchange of holes mediates ferromagnetic coupling, and long-range ferromagnetic order sets in as the Mn concentration increases.[2,3,10] This is also visible by the Mn concentration-dependent hysteresis loop changes in the inset of Fig. 7(B). On average there is much less than one hole per ferromagnetic Mn acceptor.[2,9,11] Theoretical models indicate that compensation of the negative charge for neighboring Mn-Mn pairs by up to two holes can lead to antiferromagnetic interaction between Mn neighbors.[9] It is tempting to explain the identified antiferromagnetic d^4-like Mn clusters by this scenario. The observed increase in the number of d^4-like Mn atoms by removal of Mn interstitials is in agreement with first-principles calculations that predict interstitial Mn to cluster with two or more substitutional Mn atoms.[10] This proximity of interstitial and substitutional Mn is also thought to affect the ferromagnetic coupling between the latter.[10] We surmise that this could explain the observed $12\%\pm2\%$ change in Mn magnetization upon removal of $5\%\pm1\%$ Mn interstitials. We can presently only speculate that the electric charge of substitutional Mn-Mn acceptor clusters might be screened by valence holes. Our results could then indicate that some of these holes are tightly bound around antiferromagnetic Mn-Mn pairs and may even hop onto the Mn 3*d* shell as reflected in the experimentally observed 20% reduced Mn 3*d* electron count for this species. It will be interesting to see a first-principles description of such an effect develop in the future.

V. CONCLUSION

We investigated the electronic configuration and magnetic properties of Mn impurities in GaAs depth resolved. At the surface we find an accumulation of nonferromagnetic Mn in a $3d^5$ electronic configuration. The enhanced surface segregation of this second Mn species upon annealing of the as-grown samples and the pronounced surface magnetization deficit of substitutional Mn provide strong evidence that the second Mn species is related to the diffusion of interstitial Mn. In contrast to previous studies we can exclude that the $3d^5$ configuration is only due to surface oxidation as we find a coexistence of both Mn species in the surface layer. We have shown that in the bulk of the $Ga_{1-x}Mn_xAs$ films with increasing *x* a reduction of the relative number of ferromag-

netic Mn atoms occurs. This is accompanied by an increase of antiferromagnetically ordered Mn-Mn clusters. Both Mn species are characterized by different 3*d*-electron counts. Our observations provide evidence of antiferromagnetic order in the III-V dilute magnetic semiconductor $Ga_{1-x}Mn_xAs$.

ACKNOWLEDGMENTS

We thank O. Rader and K. Fauth for helpful discussions. Further we wish to thank J. Cesar for his technical support at ID8, and the ESRF and BESSY staff for providing excellent operating conditions.

*Electronic address: kronast@bessy.de

†Permanent address: Institute of Physics, Polish Academy of Sciences, 02-668 Warszawa, Poland.

[1] H. Ohno, Science **281**, 951 (1998).

[2] C. Timm, J. Phys.: Condens. Matter **15**, R1865 (2003).

[3] S. Das Sarma, E. H. Hwang, and D. J. Priour, Jr., Phys. Rev. B **70**, 161203(R) (2004).

[4] J.-M. Tang and M. E. Flatte, Phys. Rev. Lett. **92**, 047201 (2004).

[5] S. Sanvito, P. Ordejon, and N. A. Hill, Phys. Rev. B **63**, 165206 (2001).

[6] V. F. Sapega, M. Moreno, M. Ramsteiner, L. Däweritz, and K. Ploog, Phys. Rev. B **66**, 075217 (2002).

[7] F. Maca and J. Masek, Phys. Rev. B **65**, 235209 (2002).

[8] J. Blinowski and P. Kacman, Phys. Rev. B **67**, 121204(R) (2003).

[9] Steven C. Erwin and A. G. Petukhov, Phys. Rev. Lett. **89**, 227201 (2002).

[10] P. Mahadevan and A. Zunger, Phys. Rev. B **68**, 075202 (2003).

[11] T. Dietl, H. Ohno, F. Matsukura, J. Cibert, and D. Ferrand, Science **287**, 1019 (2000).

[12] G. van der Laan and B. T. Thole, Phys. Rev. B **43**, 13401 (1991).

[13] H. Ohldag, V. Solinus, F. U. Hillebrecht, J. B. Goedkoop, M. Finazzi, F. Matsukura, and H. Ohno, Appl. Phys. Lett. **76**, 2928 (2000).

[14] S. Ueda, S. Imada, T. Muro, Y. Saitoh, S. Suga, F. Matsukura, and H. Ohno, Physica E (Amsterdam) **10**, 210 (2001).

[15] Y. Ishiwata, M. Watanabe, R. Eguchi, T. Takeuchi, Y. Harada, A. Chainani, S. Shin, T. Hayashi, Y. Hashimoto, S. Katsumoto, and Y. Iye, Phys. Rev. B **65**, 233201 (2002).

[16] Y. L. Soo, G. Kioseoglou, S. Kim, X. Chen, H. Luo, Y. H. Kao, H. J. Lin, H. H. Hsieh, T. Y. Hou, C. T. Chen, Y. Sasaki, X. Liu, and J. K. Furdyna, Phys. Rev. B **67**, 214401 (2003).

[17] K. W. Edmonds, P. Boguslawski, K. Y. Wang, R. P. Campion, S. N. Novikov, N. R. S. Farley, B. L. Gallagher, C. T. Foxon, M. Sawicki, M. Buongiorno Nardelli, and J. Bernholc, Appl. Phys. Lett. **84**, 4065 (2004).

[18] G. M. Schott, G. Schmidt, G. Karczewski, L. W. Molenkamp, R. Jakiela, A. Barcz, and G. Karczewski, Appl. Phys. Lett. **82**, 4678 (2003).

[19] K. W. Edmonds, P. Boguslawski, K. Y. Wang, R. P. Campion, S. N. Novikov, N. R. S. Farley, B. L. Gallagher, C. T. Foxon, M. Sawicki, T. Dietl, M. B. Nardelli, and J. Bernholc, Phys. Rev. Lett. **92**, 037201 (2004).

[20] D. L. Windt (unpublished).

[21] D. G. Stearns, J. Appl. Phys. **65**, 491 (1989).

[22] D. Wu, D. J. Keavney, Ruqian Wu, E. Johnston-Halperin, D. D. Awschalom, and Jing Shi, Phys. Rev. B **71**, 153310 (2005).

[23] K. M. Yu, W. Walukiewicz, T. Wojtowicz, I. Kuryliszyn, X. Liu, Y. Sasaki, and J. K. Furdyna, Phys. Rev. B **65**, 201303(R), (2002).

[24] H. A. Durr, G. van der Laan, D. Spanke, F. U. Hillebrecht, and N. B. Brookes, Phys. Rev. B **56**, 8156 (1997).

[25] D. J. Keavney, D. Wu, J. W. Freeland, E. Johnston-Halperin, D. D. Awschalom, and J. Shi, Phys. Rev. Lett. **91**, 187203 (2003).

[26] J. Okabayashi, A. Kimura, T. Mizokawa, A. Fujimori, T. Hayashi, and M. Tanaka, Phys. Rev. B **59**, R2486 (1999).

[27] C. Timm and A. H. MacDonald, cond-mat/0405484 (unpublished).

[28] G. van der Laan and I. W. Kirkman, J. Phys.: Condens. Matter **4**, 4189 (1992).

[29] M. Moreno, B. Jenichen, V. Kaganer, W. Braun, A. Trampert, L. Däweritz, and K. H. Ploog, Phys. Rev. B **67**, 235206 (2003).

[30] G. van der Laan and B. T. Thole, J. Phys.: Condens. Matter **4**, 4181 (1992).

[31] Note that the line shape in Fig. 7(A) shows that this is not a pure atomic $3d^4$ configuration (Ref. 28).

[32] B. T. Thole and G. van der Laan, Phys. Rev. B **38**, 3158 (1988).